PHYSICAL REVIEW A VOLUME 4, NUMBER 4 OCTOBER 1971

Electron Capture and Loss in Collisions of Heavy Ions with Atomic Oxygen*

H. H. Lo, L. Kurzweg, R. T. Brackman, and W. L. Fite
Department of Physics, University of Pittsburgh, Pittsburgh, Pa. 15213
(Received 20 April 1971)

Electron-capture and electron-loss cross sections for various gaseous (N^+, O^+, Ar^+, Kr^+, and Xe^+) and metallic (Al^+, K^+, Fe^+, Ba^+, and Ba^{++}) ions in collisions with atomic oxygen have been measured in the energy range 30 keV to 2 MeV. Beam-in-static-gas techniques were employed. Ions formed by an electron-impact ion source were mass selected by a rf quadrupole mass filter and were accelerated by a Van de Graaff accelerator into a fast well-collimated ion beam. This ion beam was then steered through an atomic-oxygen target chamber developed to provide a collision region containing thermally dissociated oxygen atoms in the ground state. The charge states of the emerging fast-ion beam were measured and this information along with knowledge of the atomic-oxygen-target thickness within the target chamber was used to deduce the electron-capture and electron-loss cross sections of the particular fast heavy ion on neutral atomic oxygen. Comparison with theoretical calculations and other experimental data were made where possible.

I. INTRODUCTION

Charge-changing collisions involving fast heavy atoms and ions and the atmospheric gases have long been of interest because of their bearing on range and energy loss of nuclear radiations, including fission fragments, in the air. These electron-capture and electron-loss processes assume additional importance in the upper atmosphere, because the cross sections determine the fraction of time that a given particle is either charged, and bound to a line of the earth's magnetic field, or neutral, and free to cross field lines. The distribution around the earth of particles from extraterrestrial sources, e.g., solar flares, and the loss of particles in the Van Allen radiation belts exemplify applications of electron-capture and electron-loss processes to geophysics.

A large amount of data has been gathered on charge-exchange collisions involving lighter particles (H, He, and Li) which collide with neutral atmospheric gases (H_2, N_2, and O_2) and inert gases (He, Ne, Ar, Kr, and Xe) and has been discussed in several review articles.[1-3]

In some cases atomic hydrogen (thermally produced) and atomic oxygen (produced by rf discharge) have also been used as target gases in crossed-beam experiments, notably with H^+, He^{++}, and ions of atmospheric gases.[4] Recently McClure[5] has measured cross sections for charge transfer in collisions of H^+ with H using beam-in-static-gas techniques where H^+ ions were shot through an atomic-hydrogen target chamber in which part of the hydrogen molecules were thermally dissociated into atoms.

At altitudes higher than about 100 km, the oxygen in the earth's upper atmosphere is appreciably dissociated by solar uv radiation, and the measurements of Schaefer[6] have revealed that the ratio of atomic to molecular oxygen number densities increases with height above 90 km and exceeds unity above 120 km. Knowledge of the manner in which oxygen atoms react with atmospheric and other species, charged and neutral, is therefore essential for an understanding of the upper atmosphere and of the range of fission fragments.

Because of the chemical instability of atomic oxygen, laboratory studies of collisions of charged particles with atomic oxygen have been limited to a few measurements performed by Stebbings, Smith, and Gilbody[7] and Stebbings, Smith, and Ehrhardt[8] for the atmospheric ions H^+, N^+, N_2^+, O^+, O_2^+, and NO^+ in the energy range 40 eV to 10 keV. In their experiments, crossed-beam techniques were used and slow ions arising from charge transfer between the fast-ion beam and both undissociated and partially dissociated oxygen beams were detected. About 40% of the molecules in the neutral beam was dissociated by using an electrodeless rf discharge source.

When a fast incident particle A^{i+} with a charge of $+ie$ (hereafter designated as i) collides with a stationary neutral target particles B the process can be represented by

$$A^{i+}+B\rightarrow A^{j+}+B^{n+}+(j+n-i)e\ , \tag{1}$$

where A^{j+} and B^{n+} are the fast and slow products of the collision with charges j and n, respectively. The total cross section Q_{ij}^{0n} is defined in terms of the number of fast or slow secondary particles per unit time I_j or I_n, respectively, by the expression

$$I_j(\text{or } I_n)=Q_{ij}^{0n}\,n_B I_i l\ , \tag{2}$$

where n_B is the number density of target particles B, I_i is the total number of incident particles, A^{i+}, per unit time in passage through the target, and l is the path length the projectile particles pass through the target.

Generally there are two experimental methods used for these measurements in the laboratory. In the first method, both the slow residual particles B^{n+} and the slow residual electrons formed in the collision events are collected and measured. Typically, a transverse electrostatic field (i.e., the condenser method) is applied across the fast primary particles beam A^{i+} and slow ions B^{n+} are swept to one plate of the condenser while the electrons are swept to the other. The second method involves fast particle detection in which only the fast particles A^{j+} are measured without regard to the fate of the target particle. It is the fast particle detection technique which was used in the present capture and loss measurements for collisions of fast heavy ions on atomic oxygen.

The electron-capture and electron-loss cross sections are defined by

$$\sigma_{ij} = \sum_n Q_{ij}^{0n} \tag{3}$$

and represent the cross section for the fast incident particle changing charge from i to j irrespective of the change of charge state of the originally neutral slow target particles.

Measurements of σ_{ij} are made by analyzing the charge state j of fast secondary particles after a fast beam with initial charge i traverses a gas target. In the limit of low target thickness π ($\pi = n_B l$), i.e., single-collision conditions,

$$F_j(\pi) = \sigma_{ij}\pi \ , \tag{4}$$

where F_j is the fraction of those particles incident with charge i which emerge from the target with charge j. With regard to a particular change of charge, the existence of single-collision conditions is indicated by the linear increase of the corresponding charge fraction with increasing target thickness. The target thickness is normally varied by changing the pressure in the target gas cell. Hence, the capture and loss cross sections σ_{ij} can be determined from the slope of the linear portion of the curve resulting from a plot of F_j as a function of pressure.

The purpose of the present experiment was to measure electron-capture and electron-loss cross sections for various gaseous and metallic ions in collisions with oxygen atoms over the energy range 30 keV to 2 MeV.

Beam-in-static-gas techniques were employed in this work. Ions formed by an electron-impact ion source were mass selected by a rf quadrupole mass filter and were then accelerated by a Van de Graaff generator into a fast, well-collimated ion beam. This ion beam was then steered through an atomic-oxygen-target gas chamber in which O_2 was thermally dissociated at a temperature of 2300 °K. The charge states of the emerging fast-ion beam were measured and this information along with knowledge of the atomic-oxygen target thickness within the target chamber was used to simply deduce the electron-capture and electron-loss cross sections of the particular fast ion on neutral atomic oxygen.

II. EXPERIMENTAL APPARATUS

The basic components of the apparatus included a 2-MeV Van de Graaff accelerator, ion sources, a rf quadrupole mass filter, beam deflection plates, target chamber, and detection system.

In most experiments a magnetic analysis of the beam is made after acceleration in order to select particles of the desired e/m for injection into the target chamber. However, in the case of very heavy ions traveling at MeV energies, the magnets and drift distances become inconveniently large and an alternative procedure was used to obtain purity of the primary beam in the present experiments. In this work ions produced in the ion source were mass selected by passing them through a small rf quadrupole mass filter before they had obtained appreciable energy. The selected ions were then focused and accelerated by the Van de Graaff accelerator. After acceleration, the ion beam was deflected by 2 deg some 70 cm from the target chamber. It was then collimated and entered the target chamber. The ion beam emerging from target gas was analyzed by separating the variously charged species by means of deflection in a transverse electrostatic field.

Since the pressure in the vacuum system between deflection and the target chamber was about 5×10^{-7} Torr and from the capture and loss cross sections known from the experiments investigated by Brackmann and Fite,[9] it can be assured that alterations in the ion beam constituents due to collisions in the vacuum system following electrostatic purification would be substantially less than 1%.

A. Ion Sources

1. *Gaseous Ion Source*

Figure 1 shows the schematic of the source for production of gaseous ions and shows the quadrupole mass filter used for ion selection. This electron-impact ionizer, designed originally for neutral atomic-beam detection, operates by electrons emitted from four 0.127-mm-diam tungsten filaments surrounding a cylindrical cage grid, entering the grid enclosure, and ionizing neutral gas there. The neutral gas, which was stored in a small cylinder, was introduced into the ionization region by means of a thermomechanical leak assembly.

At very low source pressures this source used in conjunction with a quadrupole mass filter tuned for a mass resolution of 40 will produce currents

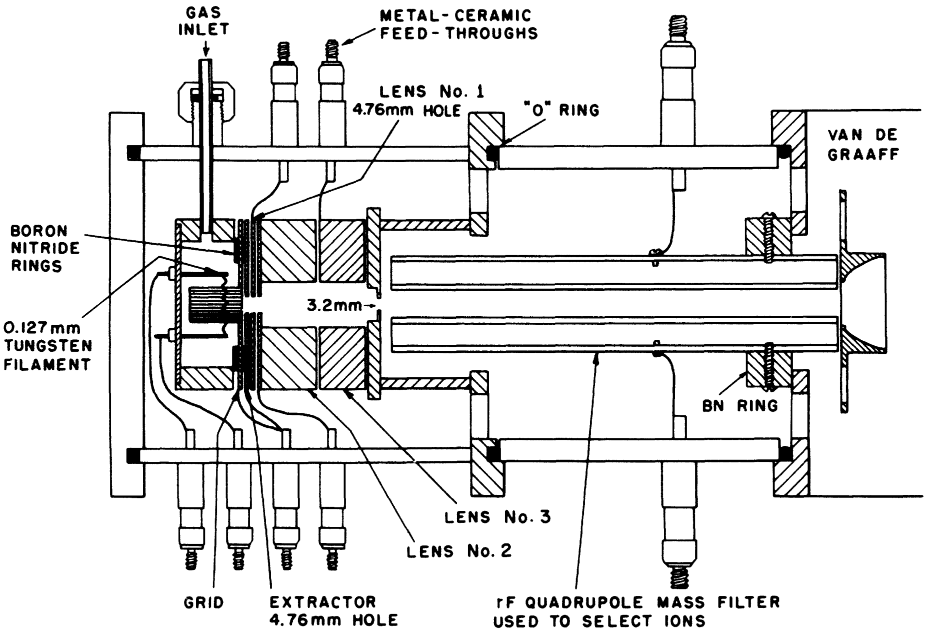

FIG. 1. Combined unit of the gaseous ion source and the rf quadrupole mass filter.

of approximately 10 mA of ions per Torr. With the source gas pressure kept below about 10^{-4} Torr, ion currents of about 10^{-7} to 10^{-8} A could be accelerated and injected through the apertures to the target chamber and collected beyond it.

With the exception of the filament power which was varied by a control rod, all other source electrodes were at fixed potentials. The source consumed about 35 W of filament power which provided an electron emission current of 50 mA with the electron energy at 92 eV. Normally, the filament and lens No. 1 were at the Van de Graaff high-voltage terminal potential, while the grid and the extractor were set at 92 V positive with respect to the filament. Lens No. 2 had a potential of 87 V positive and lens No. 3 of 450 V negative, both with respect to the filament.

The use of ion optical lenses was to focus ions into the quadrupole mass filter so that the transmission of the desired ions would be enhanced. Since even ions with the desired e/m ratio will be rejected by the filter when their initial position or initial transverse velocity component is greater than some maximum value, it is necessary to carefully focus ions into the filter.

2. *Metallic Ion Source*

The metallic ion source produced a metallic vapor which was then ionized by electron bombardment or by surface ionization. The construction of this source was similar to the one employed by Layton *et al.*[10]

Attempts were made to produce metallic ions in the ground state by operating the source with an electron energy just above the ionization potential of the element under study. Unfortunately, however, in producing Al^+ (below 195 keV), Fe^+, and Ba^{++}, higher electron energies had to be used to achieve intense enough ion beams for performing the experiments. The electron energy, i.e., the potential energy applied to the tantalum boat with respect to the tungsten filament, could be varied from 0 to 100 eV by the control system while the Van de Graaff was in operation. The electron energies used for production of metallic ions, along with the fast-ion energy ranges used, are presented in Table I.

When high electron energies (larger than the ionization potential of N_2, 15.6 eV) were used for production of Al^+, there was the certainty that N_2^+ (mass 28) formed from the ionization of background gas could not be separated from Al^+ (mass 27) by the quadrupole mass filter used in the present experiments. Therefore, the Al^+ data below 195 keV were not measured. In producing Ba^+, surface ionization from the hot filament was utilized without

TABLE I. Electron energies used for production of metallic ions.

Ion	Ion energy (keV)	Electron energy (eV)
Al^+	200–1000	11
K^+	30–1800	10
Fe^+	30–1500	43
Ba^+	30–1500	0
Ba^{++}	30–1500	28

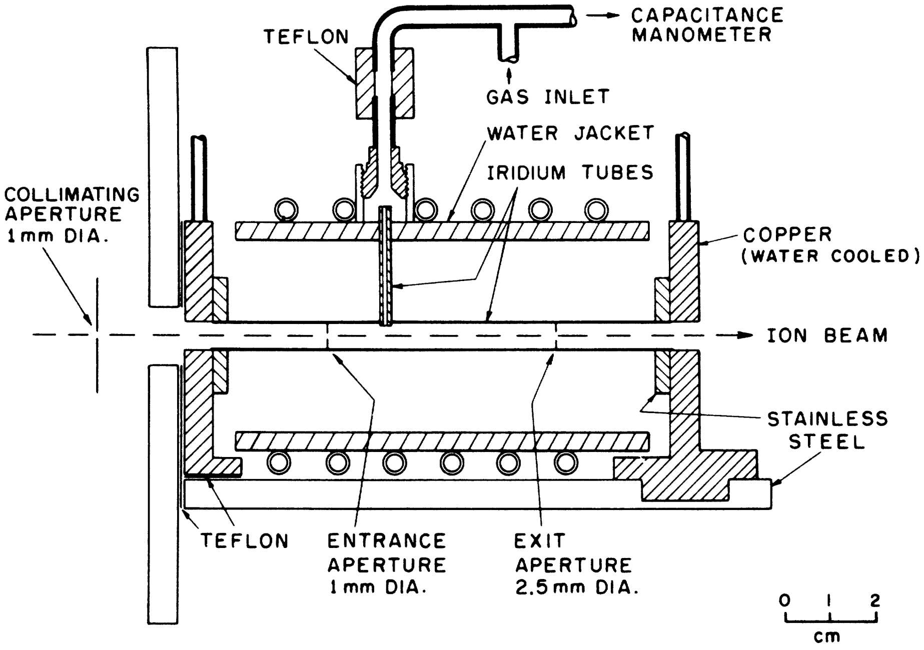

FIG. 2. Cross-section view of the atomic-oxygen target chamber assembly.

applying any electron energy, and this ensured that the Ba^+ ions were all in the ground state.

B. rf Quadrupole Mass Filter

In recent years the well-known rf quadrupole mass filter has been widely used both as an ion selector and as a residual gas analyzer in vacuum systems.

By proper choice of the physical dimensions of the quadrupole, the voltages, and the frequency, ions of unwanted charge-to-mass (e/m) ratio will undergo oscillatory trajectories of rapidly increasing amplitude and ultimately strike the electrodes, thus being removed, while desired ions will proceed with stable oscillations about the axis and finally emerge from the filter.

In this work, the quadrupole mass filter was constructed of four stainless-steel circular rods 12.7 cm long and 0.952 cm in diam. The electrodes were held in place by a boron nitride ring. The inscribed radius of the filter was 0.397 cm. The filter was located in the terminal of the Van de Graaff accelerator just in front of the focus lens of the accelerator tube. Figure 1 schematically illustrates the combined unit of the ion source and the mass filter mounted at the head of the accelerator tube.

The disadvantage of the use of a quadrupole mass filter in conjunction with metallic ion sources is that the poles, particularly near the entrance aperture, accumulate vapor depositions which eventually cause low transmission and poor ultimate resolution. Consequently, the mass spectra obtained are not as good as normally possible under more favorable conditions.

C. Atomic-Oxygen Target Chamber

1. *Construction of Target Chamber*

The atomic-oxygen target chamber illustrated in Fig. 2 was constructed of an iridium tube 10.2 cm long and 0.635 cm o.d. with a wall thickness of 0.254 mm. It was heated resistively in order to thermally dissociate the oxygen gas. An ac current of 270 A with 2.7 V across the tube raised the temperature to 2300 °K. The target chamber was measured with a Leeds and Northrup-type 8622-C optical pyrometer looking into its interior through a 0.5-mm aperture in the side of iridium tube.

A stainless-steel ring 2.54 cm o.d. was silver soldered on each end of the iridium tube and screwed on the copper block. The copper block which held the exit end was made slidable in the ion beam direction on the stainless-steel base so that it prevented the iridium tube from bending because of thermal expansion at high temperatures. The expansion along its length was noted to be about 1.5 mm at 2300 °K. A water-cooled copper jacket shielded the heat of radiation from the high-temperature target chamber. The copper tubes which carried water to cool the copper blocks also provided the electrical leads for heading the target chamber.

Oxygen gas was admitted into the central region of the target chamber, defined by two iridium buttons (each 0.051 mm thick) 5.07 cm apart, by a small side tube of iridium 2.54 cm long and 1.27 mm i.d. This small iridium tube was especially prepared using an electrical discharge machine from an iridium rod 2.36 mm o.d. The ion beam axially entered the central region through an aperture of 1 mm diam in the first of these buttons and the beam of mixed charge states emerged through the second button which has a 2.5-mm aperture.

2. *Dissociation Fraction*

Measurements employing modulated-beam techniques and quadrupole mass spectrometry were made to determine impurities and dissociation fraction within the iridium furnace. The beam effused from a 0.5-mm aperture in the side of the furnace and was mechanically chopped at 1440 Hz before entering the electron impact ionizer, the ionizer being similar to the one used for production of gaseous ions (see Fig. 1). The ions formed were then analyzed by a rf quadrupole mass filter and detected by a particle multiplier operator at 800 V. The signal from the particle multiplier was preamplified, passed through a tuned amplifier, and then passed to a phase-sensitive detector whose output was integrated and displayed on a recorder.

These measurements demonstrated that impurities were less than 2% in the atomic-oxygen signal observed and that dissociation was in excess of 99% at a temperature of 2300 °K for the maximum furnace pressure used during the experiments.

The impurities were N_2 (or CO), CO_2, H_2, Ir, and/or an oxide of iridium. These could be expected as contaminates of the tank oxygen gas used or as products of the hot furnace.

Two kinds of analysis were used to determine experimentally the dissociation fraction. The first method involved measurements of both the O^+ and the $O_2{}^+$ ion signals at a given temperature, while the second method observed the temperature dependence of the $O_2{}^+$ ion signal.

Under the condition that the mass flow of oxygen gas is constant, it is obvious that

$$N_0=\tfrac{1}{2}N_1(T)+N_2(T)\ , \tag{5}$$

where N_0 is the number of oxygen molecules per unit time entering the target chamber and $N_1(T)$ and $N_2(T)$ are the number of O and O_2 particles per unit time leaving the target chamber at temperature T, respectively. Under the same condition, the temperature dependence of the ion signal S is given by[11]

$$ST^{1/2}=\text{const}\ , \tag{6}$$

if no dissociation occurs. In order to make sure that the condition of constant mass flow holds true at different temperatures, neon gas instead of oxygen gas was admitted to the target chamber. Under the same experimental conditions, Ne signals were measured at several temperatures. The results did indicate $ST^{1/2}=\text{const}$, implying that the constant mass flow was indeed maintained at different temperatures.

Under the conditions that the gas is in thermal equilibrium, that the mass flow of gas is constant, and if the dissociation fraction D is defined as

$$D(T)=\frac{N_1(T)}{N_1(T)+2N_2(T)}\ , \tag{7}$$

then it can be shown[11] that the dissociation fraction is given by

$$D=\left[1+\sqrt{2}\,\frac{Q_1}{Q_2}\left(\frac{S_1}{S_2}-\alpha\right)^{-1}\right]^{-1}\ , \tag{8}$$

where Q_1 is the electron impact ionization cross section of oxygen atom for the process $e+O\rightarrow O^+ +2e$, Q_2 is that for the process $e+O_2\rightarrow O_2{}^+ +2e$, S_1 and S_2 are the ion currents due to ionization of atomic and molecular oxygen, respectively, and α is the ratio of S_1 and S_2 when the room-temperature target chamber issues only the molecular-oxygen beam, the atomic-oxygen signal being produced by dissociative ionization of O_2 upon electron impact. The ratio Q_1/Q_2 is available from the result of Fite and Brackmann.[12] With electron energy at 100 eV, Q_1/Q_2 has a value of 0.795.

Alternatively, it can also be shown that the dissociation fraction D' is

$$D'=1-\frac{S_2(T)}{S_0(T)}\ , \tag{9}$$

where $S_0(T)$ is the molecular signal at temperature T which would have been observed had no dissociation occurred. By using Eq. (6), Eq. (9) can be rewritten as

$$D'=1-\frac{S_2(T)}{S_2(T_0)}\left(\frac{T}{T_0}\right)^{1/2}\ , \tag{10}$$

where T_0 is any temperature at which no dissociation occurs.

Table II shows the typical data obtained for the dissociation measurements under the conditions that the electron energy was 100 eV and the O_2 number density n_2^r in the target chamber was 1.5×10^{13} molecules/cm^3 (4.7×10^{-4} Torr) at room temperature T_r. D' was calculated with $T_0=1335$ °K. It is seen that both methods give virtually complete dissociation at about 2300 °K.

Theoretically, the dissociation fraction of a gas in thermal equilibrium at temperature T can be calculated from the equilibrium constant $K_n(T)$.[13] At $T=2300$ °K, the dissociation fraction is found to be 90% when $n_2^r=1.5\times10^{13}$ molecules/cm^3. However, at the same temperature but with n_2^r five times smaller than that used above, the dissociation fraction is 97%.

When the cross-section data were taken in this work, the pressure in the target chamber decreased continuously as the reservior of the O_2 gas was

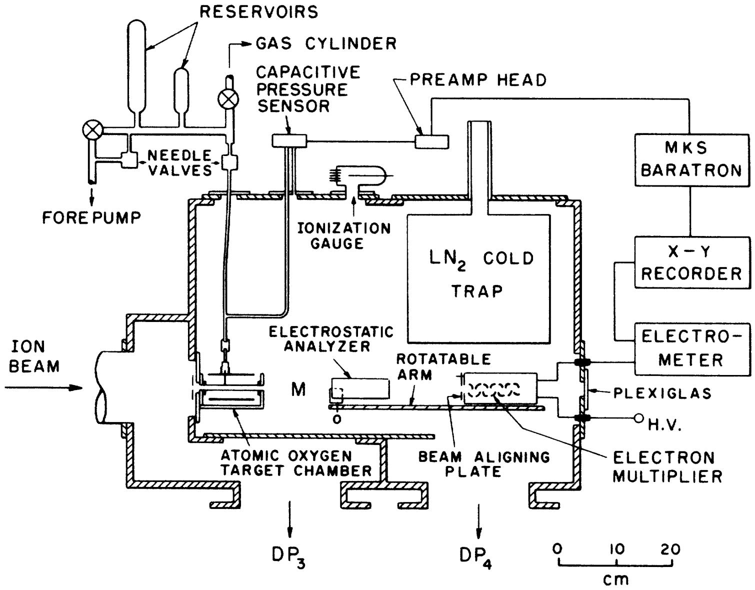

FIG. 3. Details of the target and the detection chambers. M, place to put a permanent magnet for the magnetic analysis of the ion beam; O, pivot of the rotatable arm.

slowly evacuated by an external forepump. The cross sections were evaluated using the lower pressure part as described in Sec. III. Therefore, the slight discrepancy between measured and calculated dissociation fractions within the target chamber should not constitute a problem in deducing the cross sections.

D. Ion Beam Detection

The ion beam detector used was an open electron multiplier with 14 discrete Cu-Be dynode stages (Dumont SPM 301-03-303).

The experimental setup of the apparatus in the experimental chamber of the vacuum systems is illustrated in Fig. 3. As in the experiments reported by Brackmann and Fite,[9] the detector could be rotated up to 23° from the beam direction about a pivot O which was 15 cm from the exit of target chamber and the transverse analyzing field could be varied.

A negative 1800 V was applied to the first dynode of the electron multiplier which was mounted in a grounded aluminum case. The fast-particle signals from multiplier were measured by a Keithley 600-A electrometer which then drove the Y axis of an X-Y recorder. The entrance slit of the detector was 4×9 mm with its longer dimension (in vertical direction) perpendicular to the transverse electrostatic field used to analyze the emerging ion beam.

III. EXPERIMENTAL PROCEDURES

A. Cross-Section Measurements

The fast-particle detection method was used in the electron-capture and electron-loss measurements to detect the various charge states of the fast secondary ions as they emerged from the atomic-oxygen target chamber. To detect fast neutral particles resulting from electron capture by the primary fast ions, an electric field was applied to the electrostatic analyzer (see Fig. 3) across the emerging beam to sweep away all charged particles. The rotatable arm on which the analyzer and the detector were located was lined up in the incident beam direction during the neutral-particle measurements.

In the detection of fast secondary ions of a specific charge state involving the electron loss (stripping) of primary ions, the rotatable arm was swung off the center line a few degrees and an analyzing electric field was also applied so that ions of the desired charge state were directed into the detector. In general, at a given ion energy the angle that the detector needed to be rotated to was larger for ions of a higher charge state in order to well separate them from ions in the adjacent charge states.

In essence, the purpose of the measurements was to determine the ratio of the cross sections for atomic and molecular oxygen, the ratio then being multiplied by the absolute molecular cross section in order to obtain the absolute atomic cross section at a given ion energy. The formula used can be expressed as

$$\sigma_{ij}^{(1)} = \left(\frac{n_2^r}{n_1} \frac{(dI_j^{(1)}/dp) I_i^{(2)}}{(dI_j^{(2)}/dp) I_i^{(1)}} \right) \sigma_{ij}^{(2)} , \tag{11}$$

where $\sigma_{ij}^{(1)}$ is the cross section for the fast particle changing charge from i to j in colliding with atomic-oxygen-target gas, n_1 is the atomic-oxygen number density at temperature T (where molecular-

TABLE II. Typical data in the determination of the dissociation fraction of O_2.

Temperature (°K)	O Signal S_1	O_2 Signal S_2	$S_2T_0^{1/2}$	Dissociation fraction D (%)	Dissociation fraction D' (%)[a]
300	11.5[b]	58.0	100	0	0
1335	4.60	25.0	93	0	0
1742	7.80	15.3	···	23.1	30.6
1977	17.0	9.20	···	61.5	55.5
2172	26.9	1.10	···	95.9	94.4
2262	29.0	0.10	···	99.6	99.5

[a] D' was calculated with $T_0 = 1335$ °K.

[b] $\alpha = 0.198$.

oxygen is fully dissociated), n_2^r is the molecular-oxygen number density at room temperature T_r (where molecular oxygen is undissociated), $I_i^{(1)}$ is the number of incident particles, with charge i, per unit time during the collisions with oxygen atoms, and $dI_j^{(1)}/dp$ is the slope of the curve of signal due to fast particle with charge j vs Baratron reading when the oxygen atoms are the target. Similar explanations hold true for $\sigma_{ij}^{(2)}$, $I_i^{(2)}$, and $dI_j^{(2)}/dp$ in the case of molecular-oxygen target gas. In the present case, $n_2^r/n_1 = (T/2T_r)^{1/2} = 1.96$ when the dissociation is virtually completed at 2300 °K.

A gas reservoir was filled with O_2 gas to a pressure slightly greater than 1 atm and gas flow was controlled by a needle value to maintain a target chamber pressure at room temperature of approximately 5×10^{-4} Torr. The pressure in the region between the needle valve and the small iridium tube which fed the iridium target chamber was monitored by a MKS Baratron capacitance manometer.[14] The arrangement is schematically illustrated in Fig. 3. The Baratron was calibrated using helium gas at a pressure of 10^{-3} Torr and higher against a CVC-type GM-110 McLeod gauge. The uncertainties in pressure measurements are believed to be less than ± 5%.

As indicated before, the constant mass flow of gas can be demonstrated by the constancy of a quantity $ST^{1/2}$. For the present measurement, where fast neutral atomic nitrogen was detected in the $N^+ + Ne$ charge-transfer collision, it is equivalent to state that $(dI_0/dp)T^{1/2} = \text{const}$. It was observed that the constancy of gas flow at different temperature was again ensured.

The procedure for cross-section measurements was to fill the room-temperature target chamber to a Baratron reading of 2×10^{-2} Torr after which the flow of O_2 gas into the reservoir was cut off. The reservoir was slowly evacuated through a second needle valve by an external forepump. As the reservoir was evacuated the pressure in the target chamber also diminished. The Baratron signal which was proportional to the target chamber pressure was displayed on the X axis of an X-Y recorder while the Y axis recorded the fast-particle signal. In this way a plot of signal vs pressure was obtained immediately for an incident ion beam at a given energy. From the slope of this curve on the lower pressure part and from the absolute electron-capture and electron-loss cross sections in O_2 investigated by Brackmann and Fite[9] using a conventional gas collision chamber, the correspondence between the molecular-oxygen number density in the target chamber and the Baratron reading for a given gas flow was immediately determined. The oxygen gas flow corresponding to a Baratron reading of 2×10^{-2} Torr gave an O_2 number density of about 1.5×10^{13} molecules/cm^3.

The target chamber was then heated to 2300 °K. A similar measurement procedure was then followed and plots of signal vs pressure were obtained for various charge states. Since the dissociation was complete, it was straightforward to calculate the atomic-oxygen number density n_1. From the slopes of plots, $dI_j^{(1)}/dp$, the primary ion beam currents, $I_i^{(1)}$, the n_1, and the collision length, l, the cross sections $\sigma_{ij}^{(1)}$ for the atomic-oxygen target were obtained.

B. Experimental Errors

The estimated experimental errors which are listed in Table III involved three sources: (i) a 5% uncertainty in pressure measurement of molecular oxygen using the Baratron capacitance manometer, (ii) the standard deviation of atomic-oxygen number density n_1, and (iii) the contamination of the ion beam which was determined by the magnetic analysis of the fast-ion beam as it emerged from the

TABLE III. Experimental errors (%) in electron-capture and electron-loss cross sections.

Source of error	Projectiles N^+	O^+	Ar^+	Kr^+	Xe^+	Al^+	K^+	Fe^+	Ba^+	Ba^{++}
O_2 Pressure	5	5	5	5	5	5	5	5	5	5
n_1	9	7	10	3	3	10	12	10	5	5
Beam impurity	6.5	6.5	2	2.5	2	1	0.8	1	0.6	2
SD[a] of										
Total error	12	11	11	6	6	11	13	11	7	7

[a] Standard deviation.

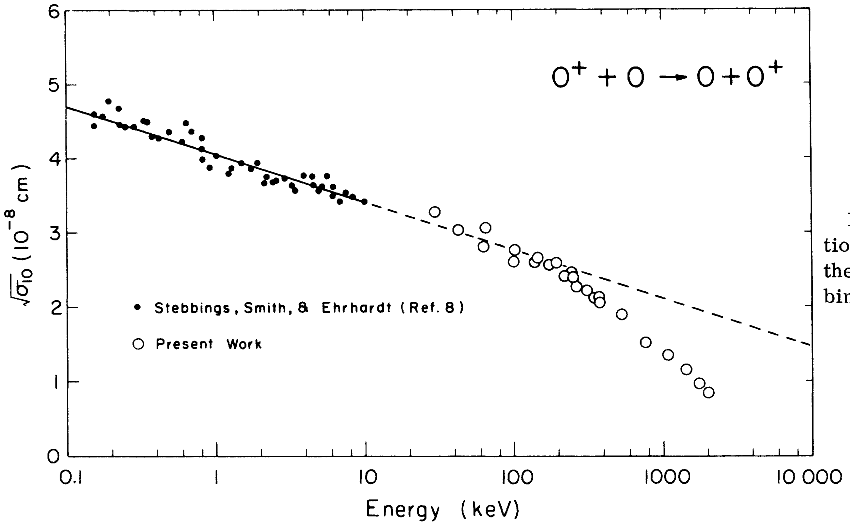

FIG. 4. Charge-transfer cross sections for O^+ in O. The dashed line is the extrapolation of the result of Stebbings *et al.* (Ref. 8).

empty target chamber. For each projectile ion, there were about 15 measured values of n_1 using the method described in the previous subsection from which (ii) was determined.

The error caused by loss of signal due to angular scattering was not investigated in this experiment. In studying collisions of Al and Fe ions and atoms with gases in the energy range 5 keV to 2.5 MeV, Layton *et al.*[10] have estimated the error to be up to 20% of the signals for the higher-stripped ions. Therefore, the data for multiple electron-loss cross sections, i.e., σ_{13}, σ_{14}, etc., should be corrected by some factor which remains yet to be further studied.

The experimental errors estimated above do not include the error caused by the effusion of the target gas through the entrance and exit apertures of the target chamber and the recombination of some effused oxygen atoms into oxygen molecules in the outer regions (2.54 cm long at both ends) of the 10.2-cm-long iridium tube where the temperatures were considerably lower. This end effect which makes the apparent cross section larger than the true cross section was estimated to be less than 8%.

IV. RESULTS AND DISCUSSION

The results for cross sections as a function of ion velocity, whose corresponding energy is scaled on the top of each figure, are shown in Figs. 4–15. Gaseous and metallic ions are grouped into two sections. Comparisons with other experimental data and theoretical calculations are made whenever they are available.

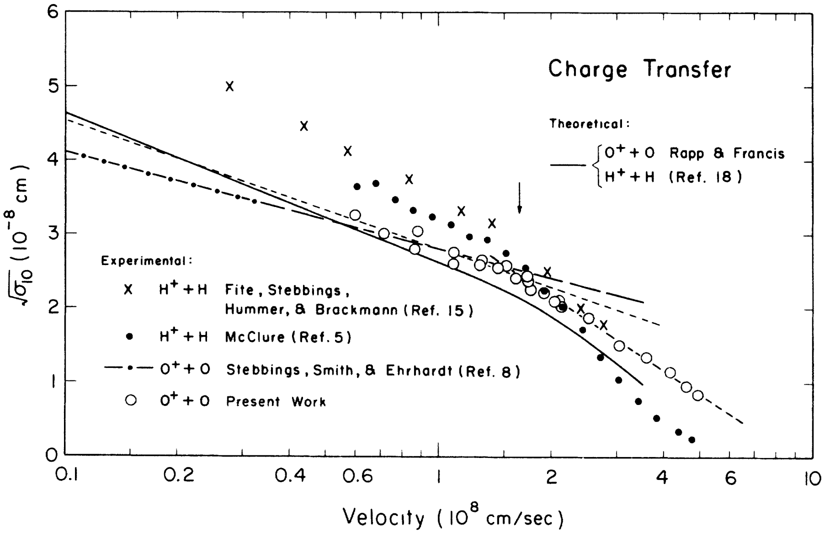

FIG. 5. Charge-transfer cross sections for $O^+ + O$ and $H^+ + H$. The deviation from the straight-line characteristic of low-energy symmetric resonant charge transfer occurs for both reactions at very nearly the same velocity which is indicated by an arrow. The long dashed line is the extrapolation of the result of Stebbings *et al.* Two short dashed lines are the least-square fit for the present work.

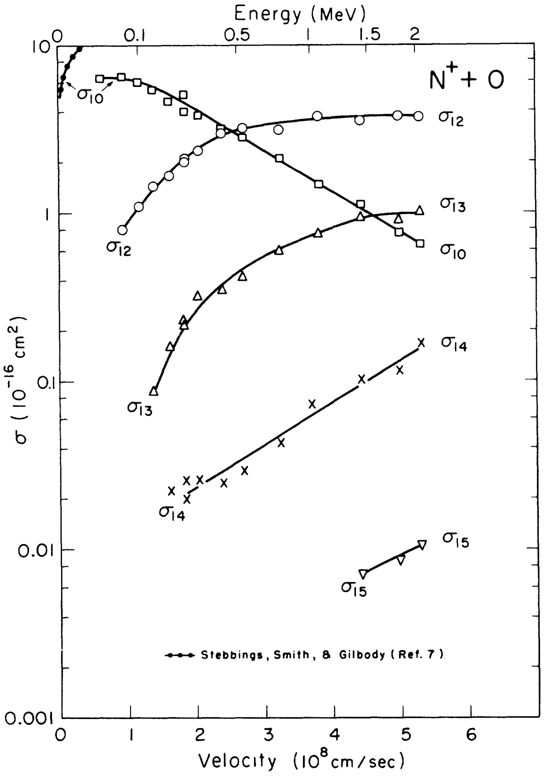

FIG. 6. Electron-capture and electron-loss cross sections for N^+ in O. The dashed curve at low energies is σ_{10} obtained by Stebbings *et al.* (Ref. 7).

A. Electron-Capture and Electron-Loss Cross Sections for Gaseous Ions

1. *Symmetric Resonant Charge Transfer in $O^+ + O$ Collisions*

Figures 4 and 5 show the results of cross sections for charge transfer σ_{10} in collisions of $O^+ + O$. Figure 4 shows a plot of $\sqrt{\sigma_{10}}$ vs $\log_{10}E$ (E is the ion energy in keV) in which the higher-energy points are from the present work and the lower-energy points are data of Stebbings, Smith, and Ehrhardt[8] who had used the slow-ion detection method in their crossed-beam experiment which had a 25% uncertainty. The two sets of data appear quite consistent.

Illustrated in Fig. 5 is a plot of $\sqrt{\sigma_{10}}$ vs $\log_{10}V$ (V is the ion velocity expressed in cm/sec) in which the result of Stebbings *et al.*[8] is again displayed. In addition, data of Fite, Stebbings, Hummer, and Brackmann,[15] using crossed-beam techniques, and McClure,[5] using beam-in-static-gas techniques, on charge transfer between proton and hydrogen atoms are also shown in Fig. 5. Fite *et al.*[15] and McClure[5] both used thermal dissociation to provide hydrogen atoms. The deviation from the straight line which is characteristic of low-energy symmetric resonant charge transfer of the form $\sqrt{\sigma_{10}} = A - B\log_{10}V$, where A and B are constants, occurs at very nearly the same velocity, $V = 1.65\times10^8$ cm/sec (220 keV for O^+), for both $O^+ + O$ and $H^+ + H$ reactions. Since ionization potentials of H and O are practically identical this similarity is not surprising.

The deviation at higher ion velocities for $H^+ + H$ charge transfer is expected by the calculation of Dalgarno and Yadav[16] using the perturbed-stationary-state method which is inadequate at high velocities of impact since it ignores transfer of momentum.

In Fig. 5 the short dashed lines which were determined by the method of least squares are given by

$$\sqrt{\sigma_{10}} = 16.57\times10^{-8} - 1.72\times10^{-8}\log_{10}V \qquad (12)$$

for ten data points at lower velocities and

$$\sqrt{\sigma_{10}} = 29.39\times10^{-8} - 3.28\times10^{-8}\log_{10}V \qquad (13)$$

for ten data points at higher velocities. It is seen from Fig. 5 that the present resonant line ($B = 1.72\times10^{-8}$ cm) given by Eq. (12) appears to be steeper than that ($B = 1.26\times10^{-8}$ cm) drawn by Stebbings *et al.*[8]

The O^+ ions used in the work of Stebbings *et al.*[8]

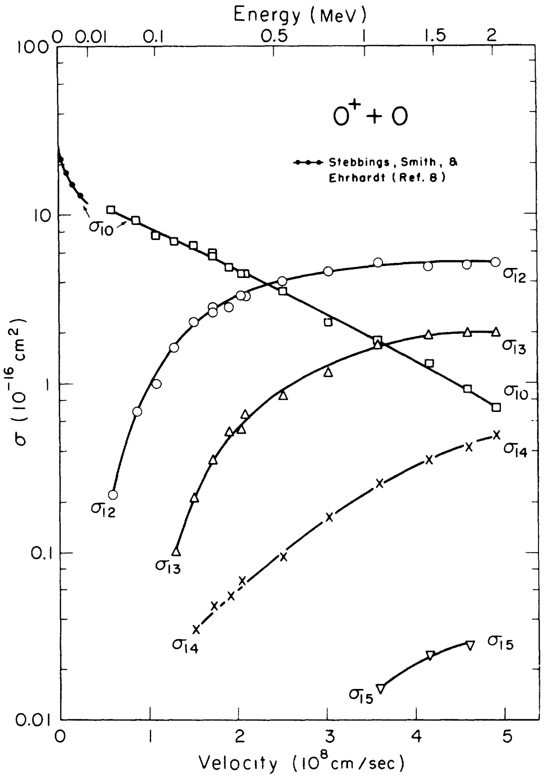

FIG. 7. Electron-capture and electron-loss cross sections for O^+ in O.

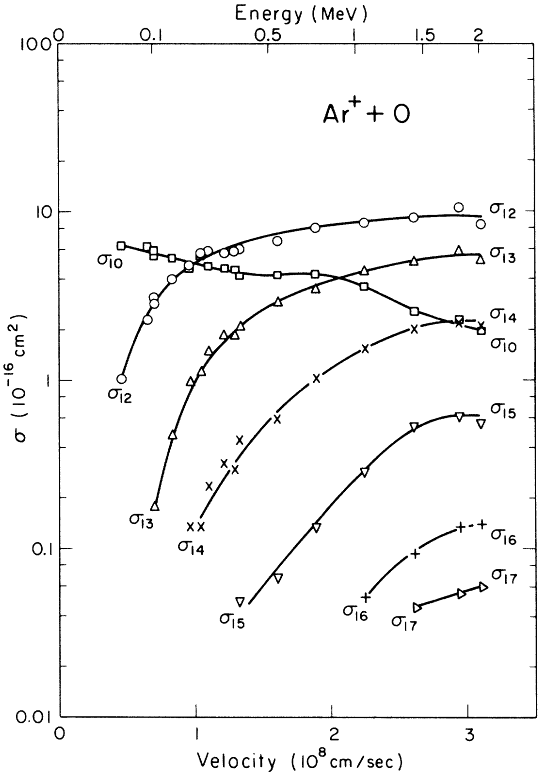

FIG. 8. Electron-capture and electron-loss cross sections for Ar^+ in O.

were obtained through dissociative ionization of molecular oxygen using 200-eV electrons as compared to 92 eV for the present work. The investigation of Turner, Rutherford, and Compton[17] has shown that electron bombardment at energies from 100 to 200 eV produced 30 to 34% of the O^+ ions in the $^2D^\circ$ metastable state, whose lifetime is of the order of hours. Therefore, the O^+ ion beams used by this work and by Stebbings *et al.*[8] contained similar excited state populations. However, their oxygen atoms being produced by a rf discharge source might have included some excited atoms which would have affected the cross sections they measured.

It is also observed that the present result for σ_{10} is in very good agreement with the theoretical value calculated by Rapp and Francis[18] for ground-state-ground-state charge transfer. The expected deviation at high velocities from the characteristic straightline is also clearly demonstrated in their curve.

2. *Capture and Loss Cross Sections*

The results for N^+, O^+, Ar^+, Kr^+, and Xe^+ gaseous ions colliding with the atomic-oxygen target gas are shown in Figs. 6–10. With the exception that cross sections for charge transfer σ_{10} for $N^+ + O$ and $O^+ + O$ collisions have been measured by Stebbings, Smith, and Gilbody[7] (SSG) and Stebbings, Smith, and Ehrhardt[8] (SSE), respectively, in the energy range 40 eV to 10 keV, no other experimental data for electron-capture and electron-loss cross sections are available for comparison. Although the energy range used by SSG[7] does not overlap with the present energy range, 30 keV to 2 MeV, it is seen from Fig. 6 that their extrapolated σ_{10} for N^+ in O at 30 keV is almost a factor of 2 larger than the present value. The $O^+ + O$ resonant case has been discussed in Sec. IV A 1.

A comparison was made between the measured $V_{\max}$, the velocity at which the maximum single-electron-capture cross section occurs, and that predicted by the near adiabatic criterion of Massey[19] in the intermediate velocity range ($10^5/\sqrt{\mu} \lesssim V \lesssim 10^8$ cm/sec, where μ is the reduced mass in amu of the collision pair),

$$V_{\max} = a|\Delta E|/h \,, \qquad (14)$$

where $|\Delta E|$ is the absolute magnitude of the energy defect for the process, h is the Planck's constant, and a is an effective-interaction distance known as the adiabatic parameter. The predicted $V_{\max}$ ultilizing the ground-state-ground-state charge-transfer energy defect and an adiabatic parameter of 7 Å[20]

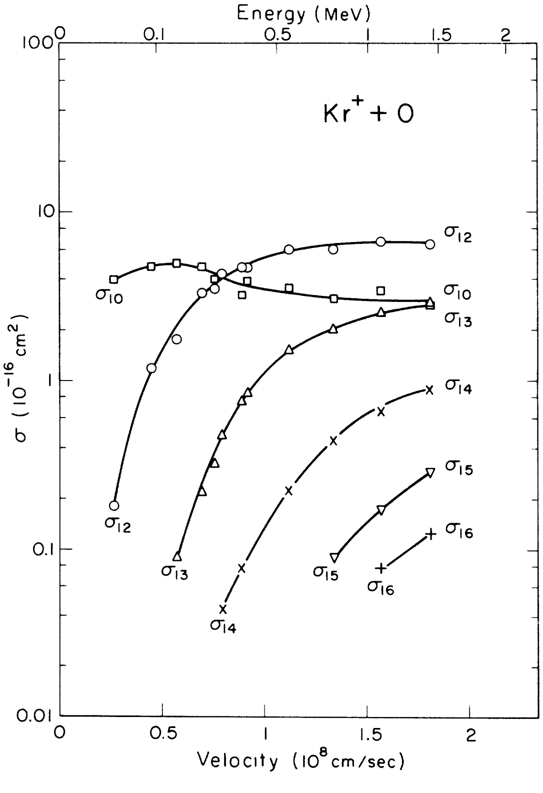

FIG. 9. Electron-capture and electron-loss cross sections for Kr^+ in O.

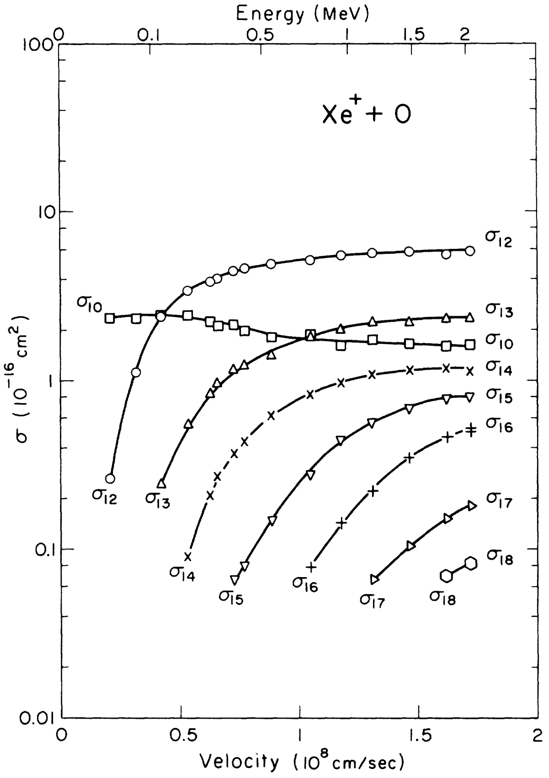

FIG. 10. Electron-capture and electron-loss cross sections for Xe^+ in O.

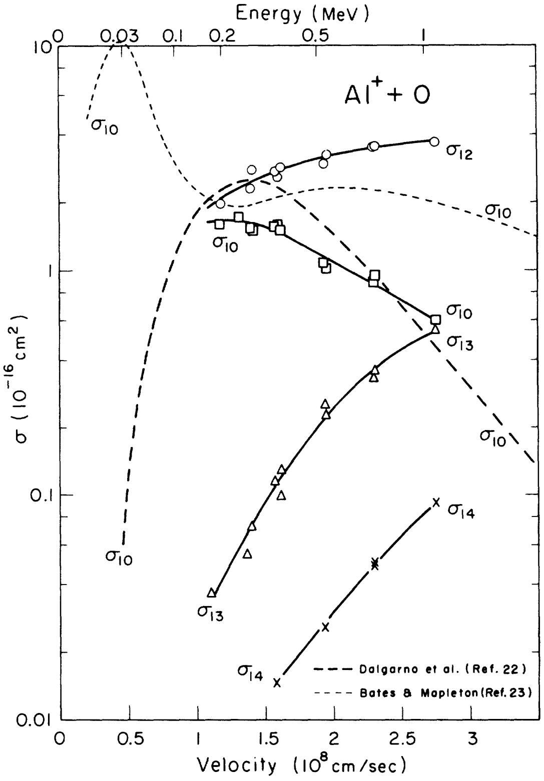

FIG. 11. Electron-capture and electron-loss cross sections for Al^+ in O. The long dashed line is σ_{10} calculated by Dalgarno *et al.* (Ref. 22). The short dashed line is σ_{10} calculated by Bates *et al.* (Ref. 23).

and the observed V_{max} are summarized in Table IV. It appears for gaseous ions that the predicted values of V_{max} are all smaller than the measured ones (except for the $O^+ + O$ symmetrical resonant case), with N^+ and Kr^+ data having profound disagreements.

The reason leading to too low an estimate of projectile velocities at which the corresponding cross sections attain their maximum could be that the values of the energy defect $|\Delta E|$ used in the Massey's criterion are simply too small, suggesting the presence of excited states either in the incident ions or in the products of reactions. The fact that the electron energy used for production of gaseous ions was 92 eV, coupled with the flight distance between the ion source and the collision region (approximately 355 cm), leads one to conclude

TABLE IV. Energy defects[a] and V_{max}[b] for charge-transfer collisions between various ions and atomic oxygen.

System	Cross section	Energy defect (eV)	V_{max} predicted (10^8 cm/sec)	V_{max} observed (10^8 cm/sec)
$N^+ + O$	σ_{10}	−0.92	0.516	~0.800
$O^+ + O$	σ_{10}	0	0	0
$Ar^+ + O$	σ_{10}	−2.15	0.363	< 0.455; 1.81
$Kr^+ + O$	σ_{10}	−0.39	0.066	0.545
$Xe^+ + O$	σ_{10}	+1.48	0.250	0.367
$Al^+ + O$	σ_{10}	+7.63	1.29	1.30
$K^+ + O$	σ_{10}	+9.27	1.57	1.50
$Fe^+ + O$	σ_{10}	+5.71	0.965	1.40
$Ba^+ + O$	σ_{10}	+8.40	1.42	~0.60; >1.50
$Ba^{++} + O$	σ_{21}	+3.61	0.608	≥1.72

[a] Energy defects were calculated for ground-state–ground-state charge transfers. "+" and "−" signs indicate endothermic and exothermic reactions, respectively. Ionization potentials were taken from Moore (Ref. 21).

[b] V_{max} is the velocity at which the maximum single-electron-capture cross secton occurs.

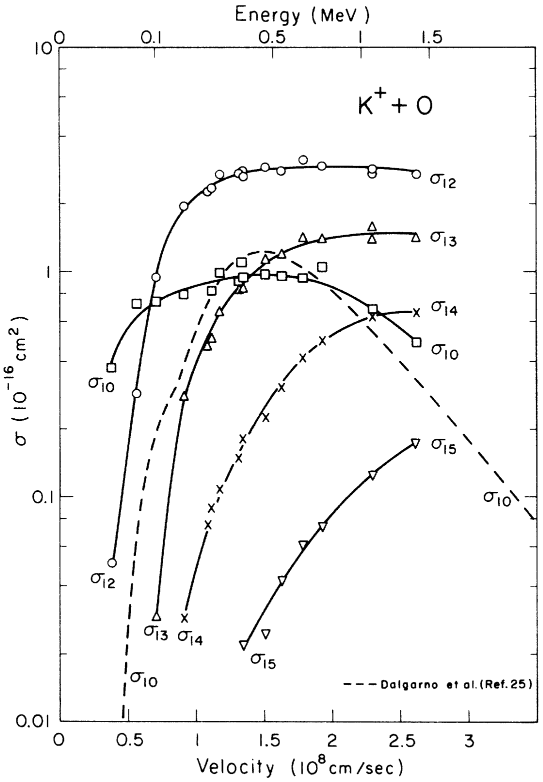

FIG. 12. Electron-capture and electron-loss cross sections for K^+ in O. The dashed line is σ_{10} calculated by Dalgarno *et al.* (Ref. 25).

that the gaseous ions used in the present work contained long-lived (lifetime greater than of the order of 10^{-6} sec) excited ions and that some of the N^+ and Kr^+ ions, in particular, were likely in highly excited states.

The appearance of second maximum in σ_{10} at about 1.81×10^8 cm/sec for $Ar^+ + O$ collisions (see Fig. 8) could be understood if a part of the slow secondary O^+ ions appeared in the excited state which would give a larger energy defect for the reaction considered.

For the gaseous ions used, σ_{12} falls off quite rapidly with decreasing energy at the lower energies, in keeping with the ions having very high second ionization potential.

B. Electron-Capture and Electron-Loss Cross Sections for Metallic Ions

The results of Al^+, K^+, Fe^+, Ba^+, and Ba^{++} in O are shown in Figs. 11-15.

It is to be noted that the Al^+ data below 1.18×10^8 cm/sec (195 keV) were not measured because, unfortunately, a usable Al^+ ion beam could not be obtained without using higher electron energies. At high electron energies the peak of N_2^+ (mass 28) would easily obscure the Al^+ (mass 27) because the quadrupole mass filter used could not quite resolve between them.

The capture cross sections σ_{10} for Al^+ and Fe^+ in O as shown in Figs. 11 and 13 are compared with theoretical calculations of Dalgarno, Florance, Macomber, and Webb[22] (DFMW) and Bates and Mapleton.[23] DFMW have calculated σ_{10} by the two-state one-electron approximation using either 1*s* or *ns* wave functions. The present experimental data are in quite good agreement with their results in predicting the location of V_{max}, the velocity at which the σ_{10} is maximum. However, the two-state theory seems to overestimate the cross section around the maximum, being about a factor of 2 too high for the case of Fe^+ (4.7×10^{-16} cm^2 by theory and 2.6×10^{-16} cm^2 by this work), and to underestimate the cross sections at velocities both above and below the V_{max}. It is to be pointed out that the two-state theory predicts similar capture cross section using either atomic or molecular oxygen as target gas because ionization potentials of O and O_2 differ only by 1.5 V (13.6 V for O and 12.1 V for O_2). Experimentally, however, the molecular-oxygen data (see Ref. 9) are always greater than atomic-oxygen data.

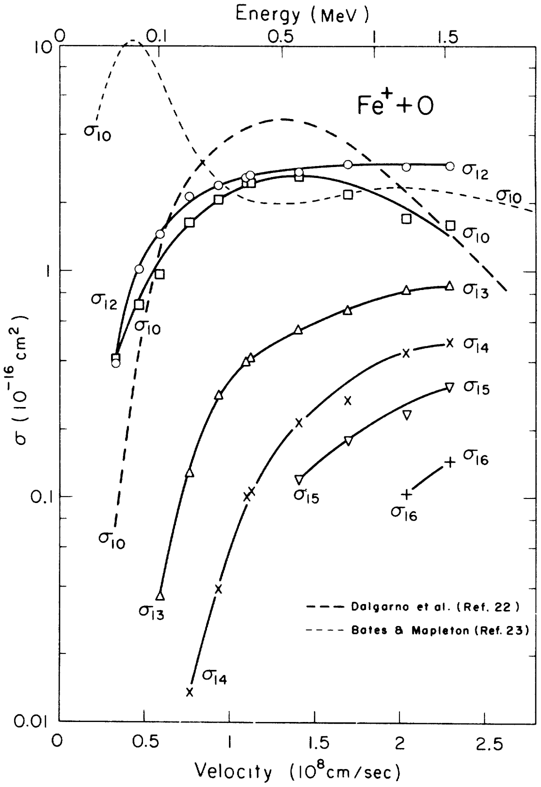

FIG. 13. Electron-capture and electron-loss cross sections for Fe^+ in O. The long dashed line is σ_{10} calculated by Dalgarno *et al.* (Ref. 22). The short dashed line is σ_{10} calculated by Bates *et al.* (Ref. 23).

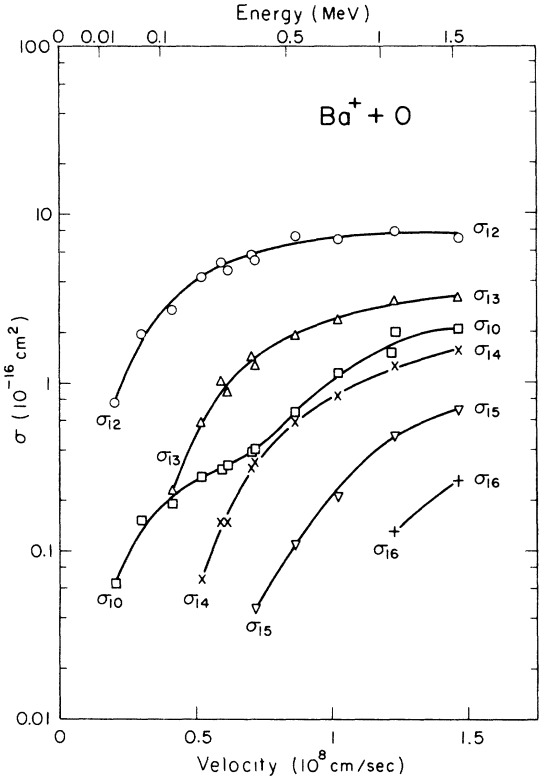

FIG. 14. Electron-capture and electron-loss cross sections for Ba^+ in O.

It is seen from Figs. 11 and 13 that except near the maximum cross sections, results calculated by Bates and Mapleton[23] using a semiclassical model, which is a modification of the classical impulse approximation of Thomas,[24] do not agree with the experimental data, their values being excessively high both in the lower- and higher-velocity regions.

The capture cross section σ_{10} for K^+ in O are compared with the theoretical result of Dalgarno, Webb, and Victor[25] (DWV) who have also used the two-state theory. The calculated cross sections have the general behavior as that predicted by DFMW.[22] For the K^+ case, however, the experimental result yields a broad maximum while the result of DWV[25] gives a fairly sharp maximum.

According to DFMW, the Rapp-Francis approximation,[18] which neglects the effect of momentum transfer, when applied without the statistical factor (the reason of replacing the statistical factor by unity has been discussed by DFMW) seems to lead to an excessively large σ_{10} at all except the lowest velocities. Thus, the cross sections for nonresonant charge transfer predicted by Rapp and Francis were not used to compare to the present results.

Referring again to Table IV, an excellent agreement is seen for metallic ions between the experimentally observed V_{max} and the theoretically predicted one, except that the latter is somewhat lower than the former for Fe^+ and Ba^{++}. The existence and lack of agreement probably can be explained by the conditions of the electron-impact ion source which have been tabulated in Table I. The Al^+ ion beam produced by an electron energy of 11 eV was primarily in the ground state because its first excited metastable state has an energy of over 4 eV. K^+ has no excited state within 20 eV of threshold, while the electron energy used in the ion source was 10 eV. Since surface ionization was utilized for producing Ba^+, the ion was certainly in the ground state. Fe^+, on the other hand, has considerable low-lying excited states within 4 eV of threshold. It is, therefore, conceivable that the Fe^+ beam contained a high excited ion population. Varying the ionization electron energy from 11 to 100 eV, a 50% increase in the cross section for σ_{10} in collisions for Fe^+ with O_2 has been observed by Fite, Layton, and Stebbings.[26]

In Fig. 14 the cross section σ_{10} for Ba^+ is found to have a principal maximum at about 1.5×10^8 cm/sec, although measurements were not made at sufficiently high velocities to fully display this peak, and a secondary structure near 6×10^7 cm/sec. The secondary structure is probably due to ionization of the atomic-oxygen target with a si-

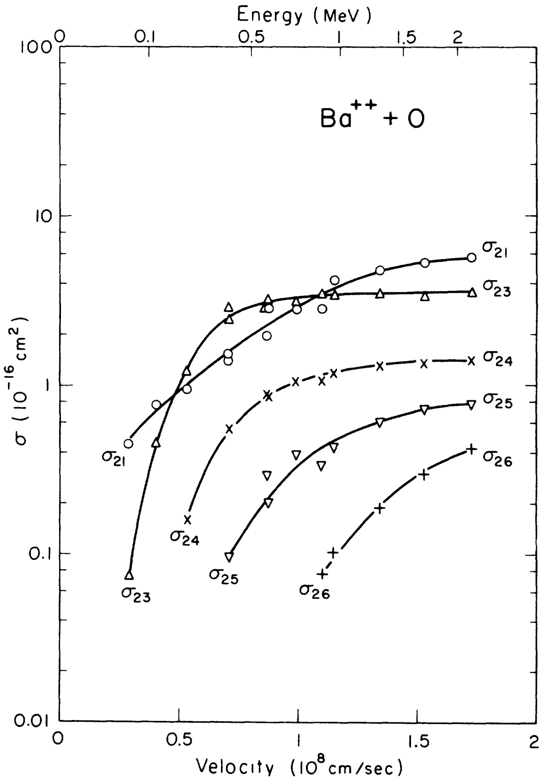

FIG. 15. Electron-capture and electron-loss cross sections for Ba^{++} in O.

multaneous excitation.

Ogurstove, Kikiani, and Flaks[27] have indicated that polarization interactions between the particles in the final states may play a role in the endothermic charge-transfer collisions of alkali metallic ions with gases in the energy range 1–30 keV. They noticed that with increasing atomic number of the alkali ion, which corresponds to increasing polarizability, the cross sections for charge transfer increased. The respective polarizabilites for potassium[28] and barium[29] are 37 and 75. Accordingly, at a given velocity, σ_{10} for Ba^+ in O should be larger than that for K^+ within the velocity range of Ogurstov *et al.*[27] It is, however, observed from Figs. 14 and 12 that the cross sections for charge transfer for Ba^+ and K^+ are about 2.0×10^{-17} and 4.3×10^{-17} cm^2, respectively, at a velocity of 4×10^7 cm/sec. This suggests that the polarization interactions do not appear to be responsible for the observed behavior of σ_{10} for Ba^+ in O. Layton[30] has reached the same conclusion as here in explaining the σ_{10} relationship between Rd^+ and Sr^+ in targets of Ar and N_2.

In the results of K^+, it is seen from Fig. 12 that σ_{12} decreases very rapidly with diminishing energy at the lower energies, in keeping with the ion having a very high second ionization potential, 31.81 V.

It is noted that the energy defect for charge transfer between Ba^+ and O ($\Delta E = 8.4$ eV) is similar to the second ionization potential of Ba ($IP_2 = 10$ eV), i.e., the energy defect for single-electron loss. However, as seen in Fig. 14, the stripping cross sections σ_{12} are substantially higher than the charge-transfer cross sections σ_{10}.

It is interesting to note in Fig. 15 that for Ba^{++} in O σ_{23} exceeds σ_{21} in the velocity region of 5×10^7 to 1×10^8 cm/sec, although the energy defect for the former process is about ten times of that for the latter one.

In Fig. 15, the cross section for the double-electron capture, σ_{20}, for $Ba^{++}+O$ is omitted because of poor reproducibility of the data.

V. CONCLUSION

The values of the electron-capture and electron-loss cross sections were measured for N^+, O^+, Ar^+, Kr^+, Xe^+, Al^+, K^+, Fe^+, Ba^+, and Ba^{++} incident on oxygen atoms in the energy range 30 keV to 2 MeV.

The present value of the cross section for charge transfer, σ_{10}, for O^+ in O appears quite consistent with that of SSE[8] whose measurement was in the energy range of 40 eV to 10 keV. The present σ_{10} is also in very good agreement with that calculated by Rapp and Francis,[18] although their prediction is for ground-state–ground-state charge transfer. It is of interest to note that in a plot of $\sqrt{\sigma_{10}}$ vs $\log_{10}V$, the deviation from the straight-line characteristic of low-energy symmetric resonant charge transfer occurs for both the $O^+ + O$ and the $H^+ + H$ reactions at very nearly the same velocity, 1.65×10^8 cm/sec, which is slightly less than the electron orbital velocity, 2.18×10^8 cm/sec, in the hydrogen atom.

It was noted that the locations of maxima of the σ_{10} curves seem to fit satisfactorily the near adiabatic hypothesis of Massey,[19] except for those incident ion species which obviously contained some excited species.

For Al^+, Fe^+, and K^+, the observed location of V_{max}, the velocity at which the σ_{10} is maximum, is in quite good agreement with that predicted by DFMW[22] and by DWV[25] using the two-state theory. However, their theory seems to overestimate the cross section around the maximum and to underestimate the cross sections at velocities both above and below the V_{max}.

Except near the maximum charge-transfer cross sections, results for Al^+ and Fe^+ in O calculated by Bates and Mapleton[23] using the semiclassical model do not agree with the present experimental data. Their values are overestimated both in the lower and higher velocity regions.

In the cases of metallic ions, σ_{12} is quite large when compared to σ_{10}. They are seen to be comparable to low energies for $Al^+ + O$ and $Fe^+ + O$. For Ba^+, σ_{12} appears to be an order of magnitude higher than σ_{10}, and only in the case of K^+ is the situation similar to that when using gaseous ions, where σ_{10} exceeds σ_{12}.

The effect of angular scattering on the higher-stripped ions was not studied in this work; therefore, it is very desirable that an investigation into this matter be conducted in the near future.

---

*This research was supported in part by the Air Force Weapons Laboratory, Air Force Systems Command, U.S. Air Force, Kirtland Air Force Base, N.M.

†Present address: Department of Physics, University of Nebraska, Lincoln, Neb. 68508.

[1] S. K. Allison, Rev. Mod. Phys. 25, 779 (1953); 30, 1137 (1958).

[2] J. B. Hasted, in *Advances in Electronics and Electron Physics*, edited by L. Marton (Academic, New York, 1960), Vol. 13, p. 1.

[3] S. K. Allison and M. Garcia-Munoz, in *Atomic and Molecular Processes*, edited by D. R. Bates (Academic, New York, 1962), Chap. 19.

[4] W. L. Fite, Ann. Geophys. 20, 47 (1964).

[5] G. W. McClure, Phys. Rev. 148, 47 (1966).

[6] E. J. Schaefer, J. Geophys. Res. 68, 1175 (1963).

[7] R. F. Stebbings, A. C. H. Smith, and H. B. Gilbody, J. Chem. Phys. 38, 2280 (1963).

[8] R. F. Stebbings, A. C. H. Smith, and H. Ehrhardt, in *Atomic Collision Processes*, edited by M. R. C. Mc-

Dowell (North-Holland, Amsterdam, 1964), pp. 814–822.

[9] R. T. Brackmann and W. L. Fite, Kirtland Air Force Base, Air Force Weapons Laboratory Technical Report No. AFWL-TR-68-96, 1968 (unpublished).

[10] J. K. Layton *et al.*, Phys. Rev. 161, 73 (1967).

[11] W. L. Fite and R. T. Brackmann, Phys. Rev. 112, 1141 (1958).

[12] W. L. Fite and R. T. Brackmann, Phys. Rev. 113, 815 (1959).

[13] U. S. JANAF Thermochemical Data, 1962, Joint Army-Navy-Air Force Thermochemical Panel, Thermal Research Laboratory, The Dow Chemical Co., Midland, Mich. (unpublished).

[14] Model 77H-10, MKS Instruments, Inc., Burlington, Mass.

[15] W. L. Fite, R. F. Stebbings, D. G. Hummer, and R. T. Brackmann, Phys. Rev. 119, 663 (1960).

[16] A. Dalgarno and H. N. Yadav, Proc. Phys. Soc. (London) A66, 173 (1953).

[17] B. R. Turner, J. A. Rutherford, and D. M. J. Compton, J. Chem. Phys. 48, 1602 (1968).

[18] D. Rapp and W. E. Francis, J. Chem. Phys. 37, 2631 (1962).

[19] H. S. W. Massey, Rept. Progr. Phys. 12, 248 (1949).

[20] J. B. Hasted, *Physics of Atomic Collisions* (Butterworths, London, 1964), Chap. 12.

[21] C. E. Moore, *Atomic Energy Levels*, Natl. Bur. Std. Circ. No. 467 (U.S. GPO, Washington, D.C., 1949, 1952 and 1958), Vols I, II, and III.

[22] A. Dalgarno, E. T. Florance, H. K. Macomber, and T. G. Webb, Kirtland Air Force Base, Air Force Weapons Laboratory Technical Report No. AFWL-TR-67-1, 1967 (unpublished).

[23] D. R. Bates and R. A. Mapleton, Proc. Phys. Soc. (London) 87, 657 (1966).

[24] L. H. Thomas, Proc. Roy. Soc. (London) A114, 561 (1927).

[25] A. Dalgarno, T. G. Webb, and G. A. Victor, Kirtland Air Force Base, Air Force Weapons Laboratory Technical Report No. AWFL-TR-68-114, 1969 (unpublished).

[26] W. L. Fite, J. K. Layton, and R. F. Stebbings, Kirtland Air Force Base, Air Force Weapons Laboratory Technical Report No. AWFL-TR-65-181, 1966 (unpublished).

[27] G. N. Ogurstov, B. I. Kikiani, and I. P. Flaks, Zh. Tekhn. Fiz. 11, 491 (1966) [Sov. Phys. Tech. Phys. 11, 362 (1966)].

[28] A. Salop, E. Pollack, and B. Bederson, Phys. Rev. 124, 1431 (1961).

[29] H. Liepack and M. Dreschler, Naturwiss. 43, 52 (1956).

[30] J. K. Layton, in *Abstracts of Papers of the Fifth International Conference on the Physics of Electronics and Atomic Collisions, Leningrad, U.S.S.R.*, 1967 (Nauka Publishing House, Leningrad, 1967), p. 412.

PHYSICAL REVIEW A VOLUME 4, NUMBER 4 OCTOBER 1971

Study of the Discrepancy between "Prior" and "Post" Approximations in Quantum Calculations of the *e*-H Excitation Cross Sections by the Correlations Method

Madeleine M. Felden and Marceau A. Felden
Laboratoire de Physique des Milieux Ionisés, 54 *Nancy, France*

(Received 23 November 1970)

In the calculation of excited-state cross sections for electron impact on hydrogen atoms, the hypothesis $A=\vec{\nabla}_1 \ln\phi_j(\vec{r}_1)\cdot(\vec{\nabla}_R \ln g_j^\pm - \vec{\nabla}_\rho \ln g_j^\pm)=0$ is used to solve the Schrödinger equation of the system. The purpose of this work is to take into account this term assuming that $\vec{\nabla}_1 \ln\phi_j(\vec{r}_1)$ is equal to a constant vector $\vec{C}_j$ dependent on the atomic state under consideration. Taking into account the justification and the consequences of this hypothesis, the equation of the system is solved when one puts the term A into this form. The transition amplitudes T_{0n} are calculated by "prior" and "post" approximations and compared, and the cross sections are obtained and discussed for four transitions. These various results show that the introduction of the term A favors the prior approximation because it is expressed by a constant modification of the incident electron energy, which is not the case for the post approximation.

I. INTRODUCTION

The excitation cross section for electron impact on a hydrogen atom from its initial state (0) to an excited state (n) is described (in the atomic unit system), the exchange being neglected, by the relation

$$\sigma_{0n}=\frac{k_n}{4\pi^2 k_0}\int |T_{0n}|^2\, d\Omega\,, \tag{1}$$

where $\vec{k}_0$ and $\vec{k}_n$ are the wave vectors of the incident and scattered electrons, and $d\Omega$ is an element of solid angle.

There are two equivalent relationships to express the transition amplitude[1]:

$$T_{0n}^{\text{prior}}=\langle\,\phi_n(\vec{r}_1)\,e^{i\vec{k}_n\cdot\vec{r}_2}\,|\,\hat{V}\,|\,\psi_0^+(\vec{r}_1,\vec{r}_2)\rangle \tag{2}$$

or

$$T_{0n}^{\text{post}}=\langle\,\psi_n^-(\vec{r}_1,\vec{r}_2)\,|\,\hat{V}\,|\,\phi_0(\vec{r}_1)\,e^{i\vec{k}_0\cdot\vec{r}_2}\rangle\,. \tag{3}$$

The interaction potential V has the value

$$V=\frac{1}{|\vec{r}_2-\vec{r}_1|}-\frac{1}{r_2}\,. \tag{4}$$

The indices 1 and 2 characterize, respectively,